Asian Journal of Chemistry; Vol. 27, No. 4 (2015), 1265-1268

ASIAN JOURNAL OF CHEMISTRY

http://dx.doi.org/10.14233/ajchem.2015.17477

Light-Emission Properties and Internal Energy Transfer Phenomenon of Calcium Zirconate Phosphor Doped with Mn^{2+}

BAI-BIN WANG and WEIN-DUO YANG*

Department of Chemical and Materials Engineering, National Kaohsiung University of Applied Sciences, No. 415, Jiangong Road, Sanmin Dist., Kaohsiung City 807, Taiwan

*Corresponding author: Fax: +886 73830674; Tel: +886 73814526, Ext 5116; E-mail: ywd@kuas.edu.tw

Received: 25 February 2014; *Accepted*: 15 May 2014; *Published online*: 4 February 2015; AJC-16772

This study employed a cellulose-citric acid method to synthesize $CaZrO_3:Mn^{2+}$ phosphor to examine the light-emission properties, as well as the distance and mechanism of energy transfer between Mn^{2+} ions. The crystal structure was analyzed using X-ray powder diffraction. The appearance and element composition of the particles were observed using a field emission scanning electron microscopy with energy-dispersive X-ray spectroscopy and the excitation and emission spectra of the phosphors were recorded using a fluorescence spectrophotometer. The results indicate that the addition of Mn^{2+} did not influence the crystal structure of $CaZrO_3:Mn^{2+}$ phosphor and light emission can be attributed to the replacement between Mn^{2+} ions and Zr^{4+} ions, forming the emission center. The maximum distance for energy transfer between Mn^{2+} ions was estimated to be 62.72 Å. Finally, the results verify Dexter's theory that the mechanism of energy transfer between Mn^{2+} ions is an electric quadrupole interaction.

Keywords: Distance for energy transfer, Mechanism of energy transfer, Electric quadrupole interaction.

INTRODUCTION

Zirconates (XYO_3; X = Sr, Ba, Ca; Y = Zr) have high resistance to corrosion, high chemical stability and high melting points, making them popular materials in the nuclear industry and metallurgy. In addition, zirconates doped with acceptor ions, such as Lu^{3+}, Y^{3+}, Gd^{3+}, Ga^{3+}, Sc^{3+} and In^{3+}, allow proton conduction at high temperatures. This attribute has wide industrial applications in hydrogen sensors, fuel cells, solid electrolytes, electronic ceramics and refractory materials[1-7].

Previously, calcium zirconate powder ($CaZrO_3$) was obtained using a conventional solid state reaction in which calcium carbonate and zirconium dioxide (ZrO_2) are ground, mixed and heated to 1850 °C[8]. However, the calcium zirconate powder derived through this method is prone to inconsistencies in particle size and clusters. Accordingly, researchers developed the cellulose-citric acid method for the synthesis of powder. Previous studies have established that adding cellulose can enhance the uniformity of positive ions mixed in solutions. Moreover, the resulting powder particles are smaller and spread more evenly. Thus, we believe that the cellulose-citric acid method could be used to resolve the issue of uneven particles and clusters in the synthesis of $CaZrO_3:Mn^{2+}$ phosphor[9,10].

However, the light-emission and energy-transfer properties of $CaZrO_3$ phosphor doped with varying quantities of Mn^{2+} have not been previously investigated. This study successfully synthesized $CaZrO_3:Mn^{2+}$ phosphor in a method using cellulose-citric acid to examine the light-emission properties of this material, as well as the distance and mechanism of energy transfer between Mn^{2+} ions.

EXPERIMENTAL

Synthesis of $CaZrO_3:Mn^{2+}$ phosphor: This study utilized a novel method using cellulose-citric acid to synthesize Mn^{2+}-doped $CaZrO_3$ phosphor. First, quantities of calcium acetate hemihydrate [$Ca(CH_3COO)_2{\cdot}0.5H_2O$] (Sigma Aldrich, 99.99 %), zirconium oxychloride octahydrate ($ZrOCl_2{\cdot}8H_2O$) (Sigma Aldrich, 99.99 %), and manganese acetate tetrahydrate [$Mn(CH_3COO)_2{\cdot}4H_2O$] (Sigma Aldrich, 99.99 %) were precisely weighed and dissolved in deionized water to obtain a clear solution containing Mn^{2+}, Ca^{2+}, and Zr^{4+} ions. Precise quantities of citric acid (Riedel-de Haën, 99.99 %) and cellulose (Alfa Aesar, 99.99 %) were added to the solution and stirred thoroughly to produce a white solution. After being stirred continuously at 75 °C for 4 h, the white solution was dried in an oven at 110 °C. The resulting powder then underwent calcination at 1200 °C for 6 h to form $CaZrO_3:Mn^{2+}$ phosphor.

The crystal structure of $CaZrO_3:Mn^{2+}$ phosphor was analyzed using X-ray powder diffraction (XRD, X' Pert PRO,

λ_{CuK_α} = 1.5406 Å, scanning rate = 4° min^{-1}, scanning range = 20° ≦ 2θ ≦ 80°) and the appearance and element composition of the particles were observed using a field emission scanning electron microscopy with energy-dispersive X-ray spectroscopy (FE-SEM/EDX, S-4700). The excitation and emission spectra of the phosphor were recorded using a fluorescence spectrophotometer (FS, Hitachi F-4500).

RESULTS AND DISCUSSION

Crystal structure and particle appearance of $CaZrO_3:Mn^{2+}$ phosphor: Fig. 1 presents the XRD images of $CaZrO_3$ phosphor with varying quantities of Mn^{2+} calcined at 1200 °C for 6 h. As shown in the figure, $CaZrO_3:Mn^{2+}$ phosphor displays a single crystalline phase. Compared with standard powder diffraction cards, the intensity of the diffraction peak was consistent with PDF card number 35-0645[11,12]. The XRD diffraction peaks for various quantities of doped Mn^{2+} were not significantly different, indicating that the doping of different Mn^{2+} contents did not influence the crystal structure of $CaZrO_3:Mn^{2+}$ phosphor. Using XRD data and XRD comparison software, $CaZrO_3:Mn^{2+}$ phosphor was found to exhibit an orthorhombic structure belonging to the Pnma{62} space group. The lattice parameters are a = 5.762 Å, b = 8.017 Å, c = 5.591 Å and the unit cell volume is V = 258.27 $Å^3$. Fig. 2 (a) presents an FE-SEM image of $CaZrO_3$ doped with Mn^{2+}, in which the particles of the phosphor appear in the form of irregular spheres. Fig. 2 (b) presents an EDX graph of $CaZrO_3$ doped with Mn^{2+}, in which the particles of the phosphor comprises Ca atoms and Zr atoms and O atoms and Mn atoms.

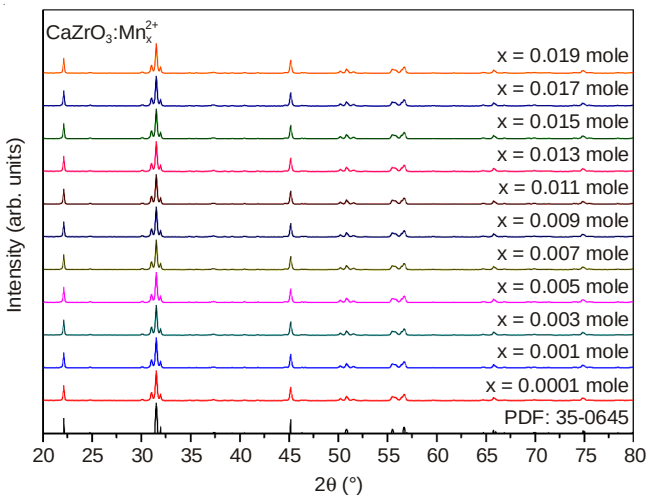

Fig. 1. XRD image of $CaZrO_3$ phosphor doped with varying quantities of Mn^{2+}

Light-emission properties of $CaZrO_3:Mn^{2+}$ phosphor: Phosphors consist primarily of a host lattice and an activator. In $CaZrO_3:Mn^{2+}$ phosphor, $CaZrO_3$ is the host lattice and Mn^{2+} is the activator. The crystal structure of $CaZrO_3$ consists of an octahedral unit formed by six O atoms and one Zr atom ($[ZrO_6]$) as well as an dodecahedral unit formed by twelve O atoms and one Ca atom ($[CaO_{12}]$)[13-19]. The radii of Mn^{2+}, Ca^{2+} and Zr^{4+} ions are 0.067 nm, 0.134 nm and 0.072 nm, respectively[20-22]. The radii of Mn^{2+} and Zr^{4+} ions are the closest, leading to an exchange of positions and the formation of the

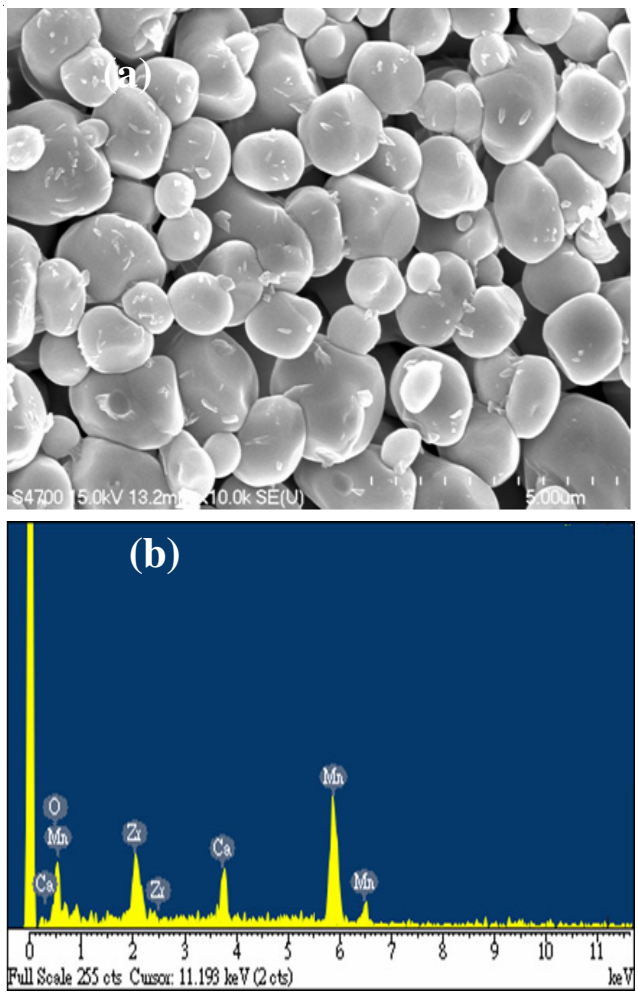

Fig. 2. FE-SEM image and EDX graph of $CaZrO_3:Mn^{2+}$ phosphor

emission center[23]. For this reason, doping the $CaZrO_3$ host lattice with Mn^{2+} ions creates a light-emitting phosphor.

Figs. 3 and 4 show that the intensity of the excitation and emission spectra of $CaZrO_3:Mn^{2+}$ phosphor vary with the amount of doped Mn^{2+}. In Fig. 4, the maximum intensity of emission occurs at a Mn^{2+} doping of 0.001 mole; as the Mn^{2+} doping increases the intensity decreases, with the critical content, or quench threshold, of Mn^{2+} doping being 0.001 mole. From Figs. 3 and 4, it is apparent that $CaZrO_3:Mn^{2+}$ phosphor is excited by light with a wavelength of 457 nm, emitting light with a wavelength of 541 nm. Based on the energy levels of Mn^{2+} ions[24-28], an excitation wavelength of 457 nm corresponds to the $^6A_1(^6S) \rightarrow {}^4T_2(^4G)$ transition[29,30] and an emission wavelength of 541 nm corresponds to the $^4T_1(^4G) \rightarrow {}^6A_1(^6S)$ transition[29,30].

Energy-transfer properties of $CaZrO_3:Mn^{2+}$ phosphor: To understand the energy transfer mechanism in $CaZrO_3:Mn^{2+}$ phosphor, the theories of Blasse and Dexter were employed to calculate the energy-transfer distance and verify the energy transfer mechanism between Mn^{2+} ions.

An increase in doping content causes the Mn^{2+} ions to become more densely packed, resulting in the transfer of energy between them. The close distance between the ions under such conditions is referred to as the energy transfer distance; the distance at which the maximum intensity of light emission peaks in the phosphor is defined as the maximum

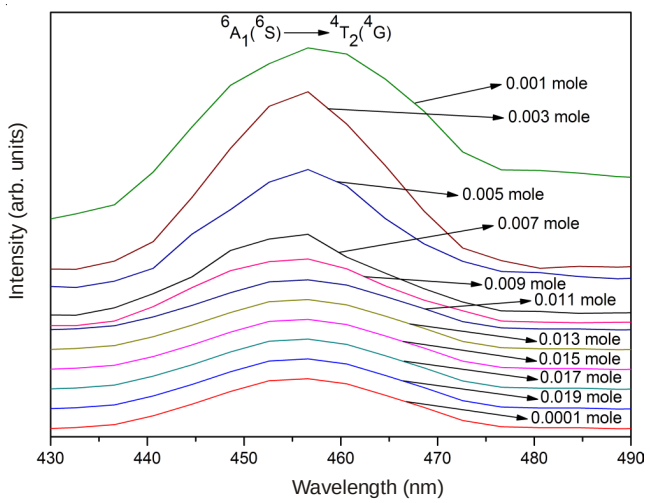

Fig. 3. Excitation spectra of $CaZrO_3:Mn^{2+}$ phosphors (Mn^{2+} content: 0.0001 mole, 0.001 mole, 0.003 mole, 0.005 mole, 0.007 mole, 0.009 mole, 0.011 mole, 0.013 mole, 0.015 mole, 0.017 mole, 0.019 mole)

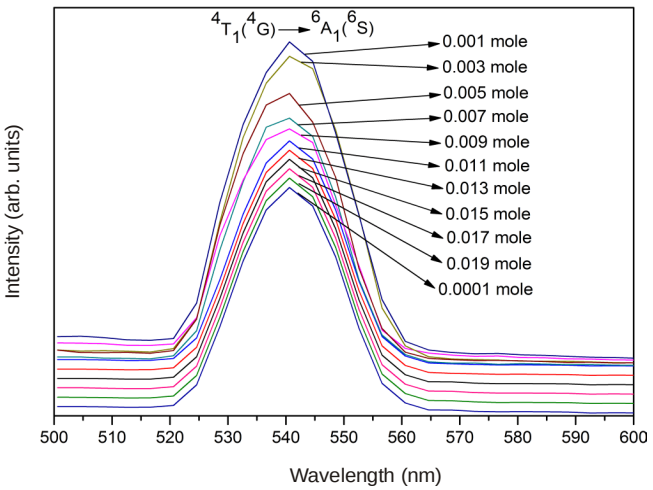

Fig. 4. Emission spectra of $CaZrO_3:Mn^{2+}$ phosphors (Mn^{2+} content: 0.0001 mole, 0.001 mole, 0.003 mole, 0.005 mole, 0.007 mole, 0.009 mole, 0.011 mole, 0.013 mole, 0.015 mole, 0.017 mole, 0.019 mole)

transfer distance. The content that contributes to this maximum value is the quench threshold. In Fig. 4, emission intensity peaks at a Mn^{2+} doping level of 0.001 mole, which represents the quench threshold. The maximum value can be calculated using Blasse's formula[31,32]:

$$\left(\frac{R_M}{2}\right)^3 \approx \frac{3V}{4\pi x_c N} \quad (1)$$

where x_c is the critical content of the activator; N is the number of sites per unit cell that the Mn^{2+} ion can occupy and V is the unit cell volume. By substituting the known values into the equation ($x_c = 0.001$ mol, N = 2, V = 258.27 Å^3), the maximum distance for the transfer of energy (R_M) between Mn^{2+} ions was calculated to be 62.72 Å.

Dexter's theory states that if energy transfer occurs between the same type of activator ions, the energy transfer mechanism can be determined by the intensity of the emission spectra. Dexter's equation is as follows[33,34]:

$$\frac{I}{x} \approx \xi\left(1 + \mu(x)^{\frac{\omega}{3}}\right)^{-1} \quad (2)$$

where I is the luminous intensity of the phosphorus material, x is the content of the activator ion and ω is the evaluation parameter of the energy-transfer mechanism between the activators. An ω value equal to 6 indicates electric dipole interaction, an ω value equal to 8 indicates electric dipole and electric quadrupole interaction and an ω value equal to 10 indicates electric quadrupole interaction. The parameters ξ and μ are constants in identical host lattice structures under identical excitation conditions. When, $\mu(x)^{\frac{\omega}{3}} \gg 1$, eqn. 2 can be simplified to eqn. 3, in which parameter ξ′ is a constant.

$$\frac{I}{x} \approx \xi'\left(\mu(x)^{\frac{\omega}{3}}\right)^{-1} \quad (3)$$

Fig. 4 shows that the critical content of Mn^{2+} in $CaZrO_3:Mn^{2+}$ phosphor is 0.001 mole. Fig. 5 is the slope map of log ($I/x_{Mn^{2+}}$) and log ($x_{Mn^{2+}}$) for a Mn^{2+} content greater than 0.001 mole in Fig. 4, displaying a straight line with a slope of -ω/3. From Fig. 5, the ratio of log ($I/x_{Mn^{2+}}$) to log($x_{Mn^{2+}}$) is constant with a slope of -3.636. Therefore, ω = 10.908, which is close to 10. This shows that the energy transfer mechanism between Mn^{2+} ions in $CaZrO_3:Mn^{2+}$ phosphor is electric quadrupole interaction.

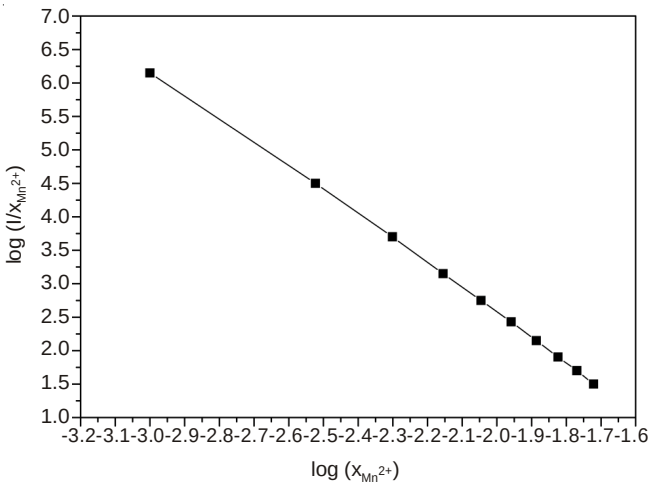

Fig. 5. log ($I/x_{Mn^{2+}}$)-log($x_{Mn^{2+}}$) relationship in $CaZrO_3:Mn^{2+}$ phosphor with Mn^{2+} content exceeding quenching threshold

Conclusion

This study successfully synthesized $CaZrO_3$ phosphor doped with Mn^{2+} in a method that employed cellulose-citric acid. XRD analysis confirmed the crystal structure of $CaZrO_3:Mn^{2+}$ phosphor as orthorhombic structure, belonging to the Pnma{62} space group. FE-SEM/EDX analysis revealed the appearance and element composition of $CaZrO_3:Mn^{2+}$ particles. From a structural perspective, the light emitted by $CaZrO_3:Mn^{2+}$ phosphor can be attributed to replacement between Mn^{2+} ions and Zr^{4+} ions, forming the emission center. The excitation spectrum presented an excitation peak at a wavelength of 457

nm, corresponding to the $^6A_1(^6S) \rightarrow {}^4T_2(^4G)$ transition in Mn^{2+} ions. The emission spectrum exhibits a peak emission at 541 nm, corresponding to the $^4T_1(^4G) \rightarrow {}^6A_1(^6S)$ transition in Mn^{2+} ions. The maximum distance for energy transfer between Mn^{2+} ions was estimated to be 62.72 Å. Finally, energy transfer between Mn^{2+} ions was found to result from electric quadrupole interactions.

ACKNOWLEDGEMENTS

The authors gratefully acknowledge the financial support of the National Science Council of Taiwan (NSC 102-2221-E-151-041-).

REFERENCES

1. T. Higuchi, S. Yamaguchi, K. Kobayashi, S. Shin and T. Tsukamoto, *Solid State Ionics*, **162-163**, 121 (2003).
2. O. Kamishima, Y. Abe, T. Ishii, J. Kawamura and T. Hattori, *Solid State Ionics*, **177**, 2375 (2006).
3. R.B. Cervera, Y. Oyama, S. Miyoshi, K. Kobayashi, T. Yagi and S. Yamaguchi, *Solid State Ionics*, **179**, 236 (2008).
4. E.K. Keler and A.K. Kuznetsov, *Zh. Prikl. Khim.*, **34**, 2146 (1967).
5. K.L. Smith, M. Colella, R. Cooper and E.R. Vance, *J. Nucl. Mater.*, **321**, 19 (2003).
6. D. de Ligny and P. Richet, *Phys. Rev. B*, **53**, 3013 (1996).
7. M.M. Sinha and A. Sharma, *Asian J. Chem.*, **21**, S108 (2009).
8. M.R. Nadler and E.S. Fitzsimmons, *J. Am. Ceram. Soc.*, **38**, 214 (1955).
9. Z. Shao, G. Xiong, Y. Ren, Y. Cong and W. Yang, *J. Mater. Sci.*, **35**, 5639 (2000).
10. Z. Shao, G. Li, G. Xiong and W. Yang, *Powder Technol.*, **122**, 26 (2002).
11. L.M. Kovba and V.K. Trunov, Rentgenofazovyi analiz (X-ray Powder Diffraction Analysis). Mosk. Gos. Univ., Moscow (1969).
12. L.M. Kovba, Rentgenografiya v neorganicheskoi khimii: Uchebnoe posobie (Textbook on X-ray Diffraction Analysis in Inorganic Chemistry). Mosk. Gos. Univ., Moscow (1991).
13. F.S. Galasso, Structure and Properties of Inorganic Solids, Pergamon Press, New York (1970).
14. P. Stoch, J. Szczerba, J. Lis, D. Madej and Z. Pedzich, *J. Eur. Ceram. Soc.*, **32**, 665 (2012).
15. M.S. Islam, R.A. Davies and J.D. Gale, *Chem. Mater.*, **13**, 2049 (2001).
16. H.J.A. Koopmans, G.M.H. van de Velde and P.J. Gellings, *Acta Crystallogr. C*, **39**, 1323 (1983).
17. B.N. Arzamasov, V.A. Brostrem and N.A. Bushe, Structural Materials: Handbook. Mashinostroenie, Moscow (1990).
18. W.D. Kingery, H.K. Bowen and D.R. Uhlmann, Introduction to Ceramics, Wiley-Interscience, New York (1976).
19. Z.L. Wang and Z.C. Kang, Functional and Smart Materials: Structural Evolution and Structure Analysis. Plenum Press, New York (1998).
20. R.D. Shannon, *Acta Crystallogr. A*, **32**, 751 (1976).
21. R.D. Shannon and C.T. Prewitt, *Acta Crystallogr. B*, **25**, 925 (1969).
22. R.D. Shannon and C.T. Prewitt, *Acta Crystallogr. B*, **26**, 1046 (1970).
23. W.D. Callister and D.G. Rethwisch, Fundamentals of Materials Science and Engineering: An Integrated Approach, Wiley, New York (2012).
24. D. Curie, C. Barthou and B. Canny, *J. Chem. Phys.*, **61**, 3048 (1974).
25. S. Koide and M.H.L. Pryce, *Philos. Mag.*, **3**, 607 (1958).
26. A.K. Mehra, *J. Chem. Phys.*, **48**, 4384 (1968).
27. L.L. Lohr, *J. Chem. Phys.*, **45**, 3611 (1966).
28. S. Shionoya and W.M. Yen, Phosphor Handbook. CRC Press, Boca Raton (1999).
29. M. Tamatani, *Jpn. J. Appl. Phys.*, **13**, 950 (1974).
30. P.I. Paulose, G. Jose, V. Thomas, N.V. Unnikrishnan and M.K.R. Warrier, *J. Phys. Chem. Solids*, **64**, 841 (2003).
31. G. Blasse, *Phys. Lett. A*, **28**, 444 (1968).
32. G. Blasse, *J. Solid State Chem.*, **62**, 207 (1986).
33. D.L. Dexter and J.H. Schulman, *J. Chem. Phys.*, **22**, 1063 (1954).
34. D.L. Dexter, *J. Chem. Phys.*, **21**, 836 (1953).